Supporting Information

For

Double protected all-inorganic perovskite nanocrystals by crystalline matrix and silica for triple-modal anti-counterfeiting codes

Leimeng Xu [#], Jiawei Chen[#], Jizhong Song[*], Jianhai Li, Jie Xue, Yuhui Dong, Bo Cai, Qingsong Shan, Boning Han, Haibo Zeng[*]

MIIT Key Laboratory of Advanced Display Materials and Devices
Institute of Optoelectronics and Nanomaterials
Herbert Gleiter Institute of Nanoscience
School of Materials Science and Engineering
Nanjing University of Science and Technology, Nanjing 210094, China

Email address: Haibo Zeng: zeng.haibo@njust.edu.cn (corresponding author)
Jizhong Song: songjizhong@njust.edu.cn (corresponding author)

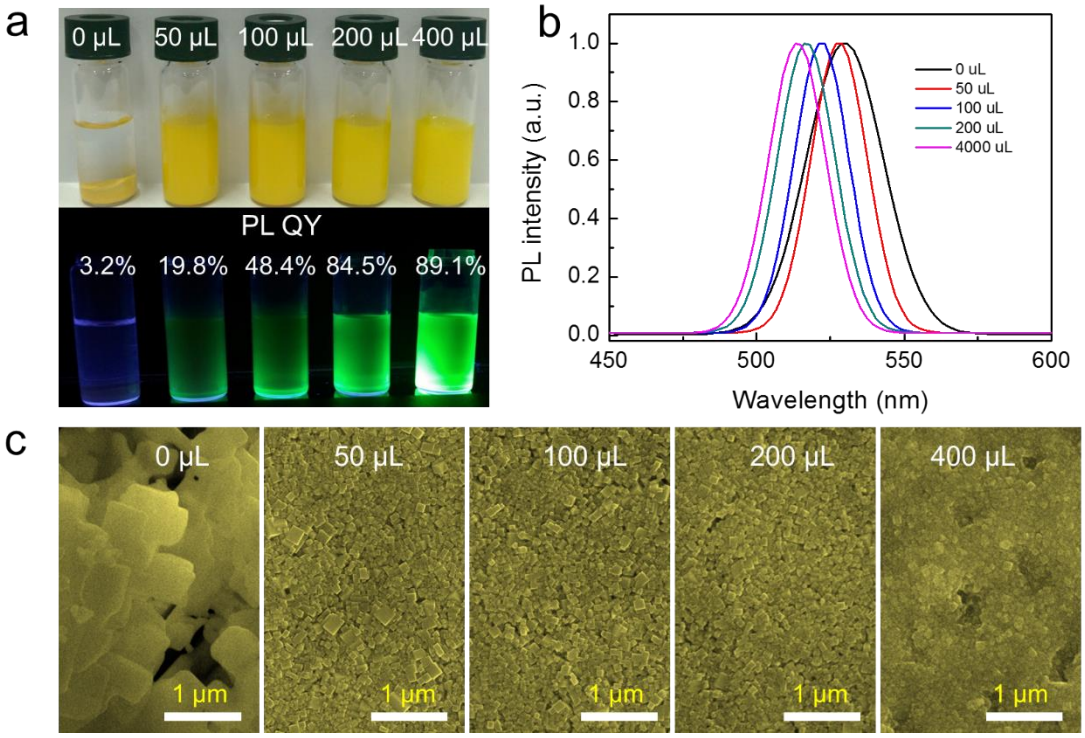

Figure S1. The effect of surfactant concentration on the dimension and PL properties of cesium lead halide NCs: (a) photographs of the NC inks with different surfactant concentration; (b) PL spectra of corresponding NCs; (c) SEM images of corresponding NCs

The NCs was synthesized as follows: the DMSO precursor solution was prepared by dissolving 0.16 mmol CsBr, 0.2 mmol $PbBr_2$ in 5 mL DMSO solvent and sonicated until a transparent solution was formed. 1 mL of DMSO precursor solution was injected into 20 mL toluene with equimolar OAm and OA (0, 50, 100, 200, 400 μL) at room temperature with the reaction time of 10 s. the SEM images of NCs was obtained by centrifugal casting on Si substrates.

The figure S1a shows the photographs of the NC inks. Without the surfactant of OAm and OA, the particle is very large, and the PL emission is very weak. With an increase in the surfactant concentration, the PL properties was evidently enhanced, and the PL QY reached 84.5% under the concentration of 200 μL. With a further increase in the surfactant concentration up to 400 μL, the PL QY has no any evident changes.

The PL spectra (Fig. S1b) of NCs have a slight blueshift along the increase surfactant concentration, which also indicated reduce of dimension.

Furthermore, the SEM images (Fig. S1c) exhibited the particle is evidently reduced after adding the surfactants. While the morphology has no obvious changes after the concentration reached 200 μL. We choose the concentration of 200 μL as the reference to study the NCs/SiO_2 composites.

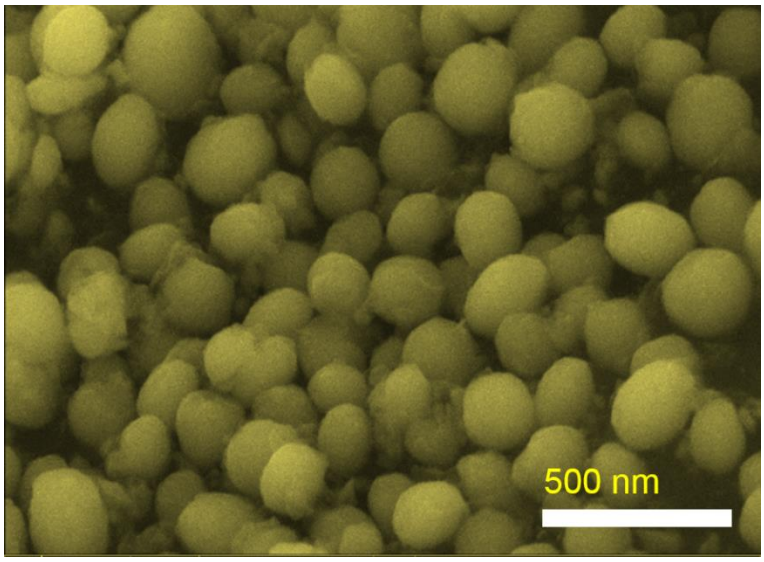

Figure S2. The large scale SEM images of spherical $CsPbBr_3@Cs_4PbBr_6/SiO_2$ NCs

The as-prepared $CsPbBr_3@Cs_4PbBr_6/SiO_2$ NCs are almost spherical with uniform size and morphology.

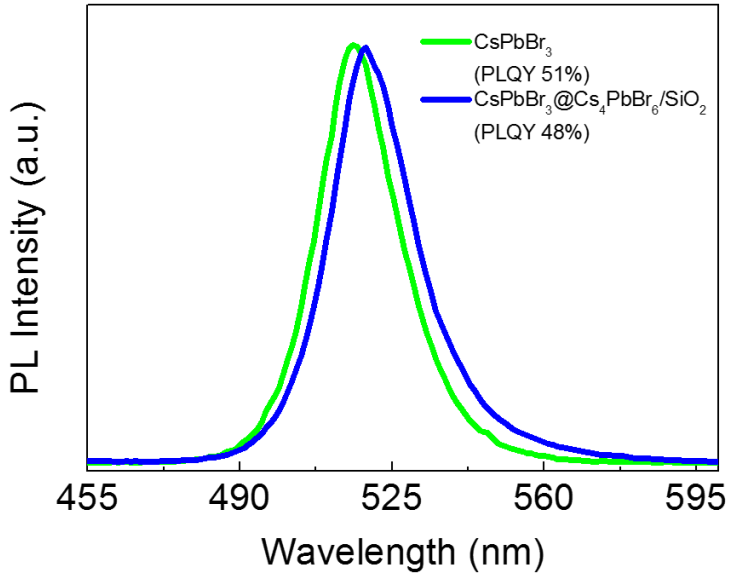

Figure S3. The comparison of the PL spectra of pure $CsPbBr_3$ NCs and $CsPbBr_3@Cs_4PbBr_6/SiO_2$ composites.

Both the pure $CsPbBr_3$ NCs and $CsPbBr_3@Cs_4PbBr_6/SiO_2$ composites exhibit the high PL QY. The $CsPbBr_3@Cs_4PbBr_6/SiO_2$ composites have a blue shift compared to $CsPbBr_3$ NCs, which may be attributed to the size effect.

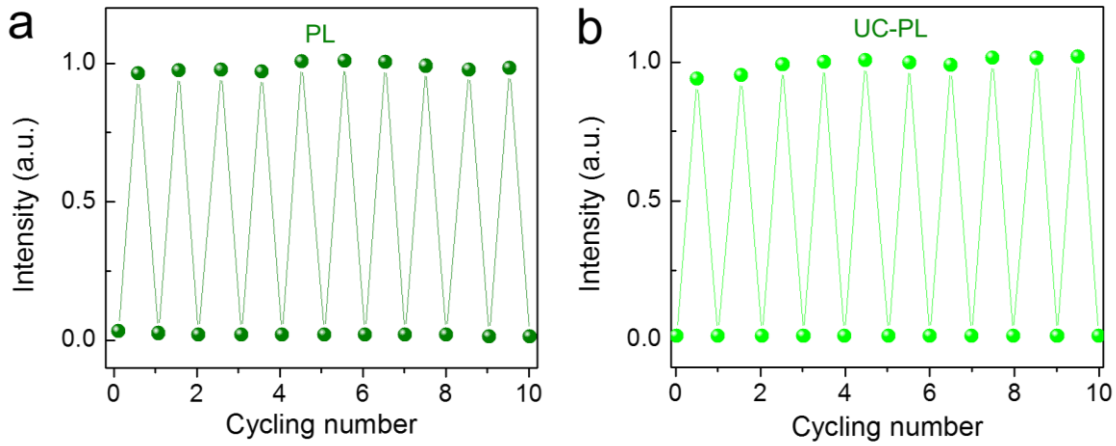

Figure S4. Reversible PL (a) and UC-PL (b) changes of the $CsPbBr_3@Cs_4PbBr_6/SiO_2$ composite film between dark and excitation with 325 nm light sources, and an 800 nm femtosecond pulse laser, respectively.

Both the PL and UC-PL properties of the $CsPbBr_3@Cs_4PbBr_6/SiO_2$ composite film exhibit the excellent reversible features.

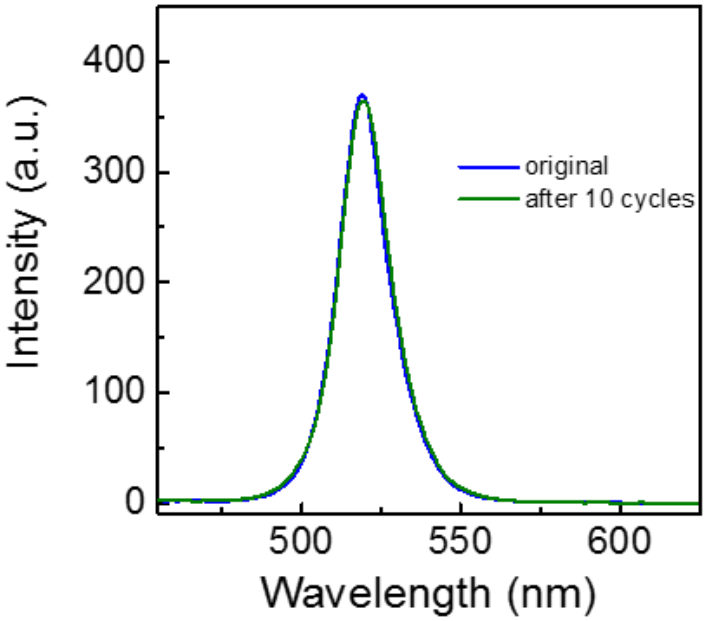

Figure S5. PL spectra of $CsPbBr_3@Cs_4PbBr_6/SiO_2$ composites before and after heating-cooling for 10 cycles between 150 ^{o}C and 30 ^{o}C.

Fig. S5 shows the changes in PL intensity for heating and cooling processes. From the 10th cycle, the luminescence intensity for heating and cooling processes is almost identical and the process is fully reversible for several heating and cooling cycles.

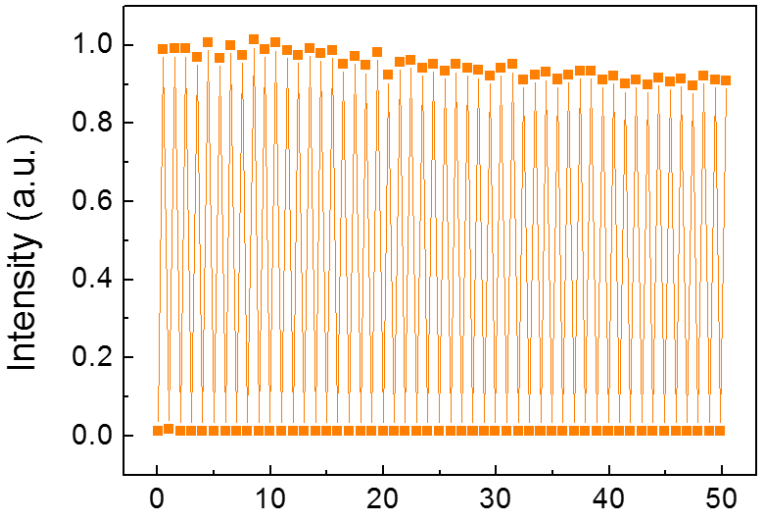

Figure S6. Reversible fluorescent response of 50 consecutive cycles at 30-150 °C of $CsPbBr_3@Cs_4PbBr_6/SiO_2$

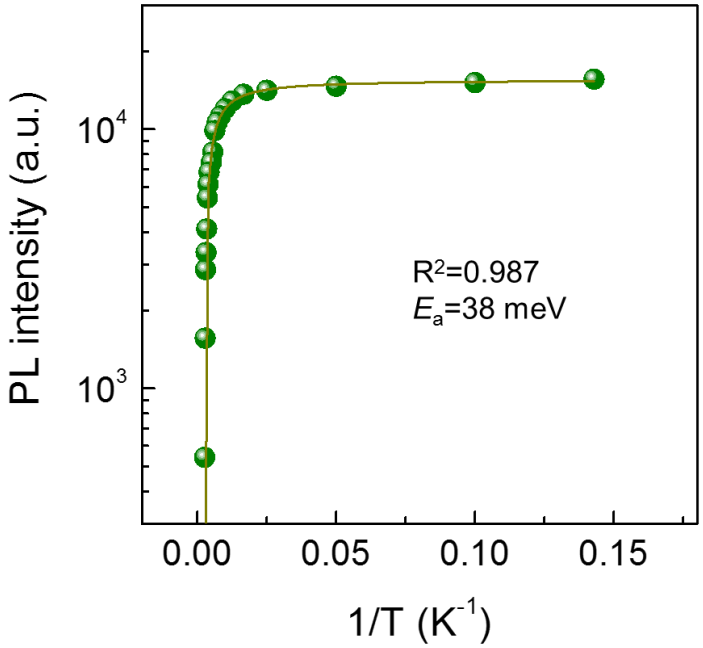

Figure S7. Arrhenius plots for PL integrated intensities for composite films from 7 to 420 K.

In order to investigate the nonradiative relaxation processes in NCs, we analyzed the quenching of the integrated PL intensity with a specific temperature. The temperature-dependent integrated PL intensity is plotted in Figure S6. The integrated PL intensity slightly changes as the temperature increases from 80 K up to 200 K. The change in the PL intensity as a function of temperature can reflect the decrease of the temperature- dependent nonradiative recombination.

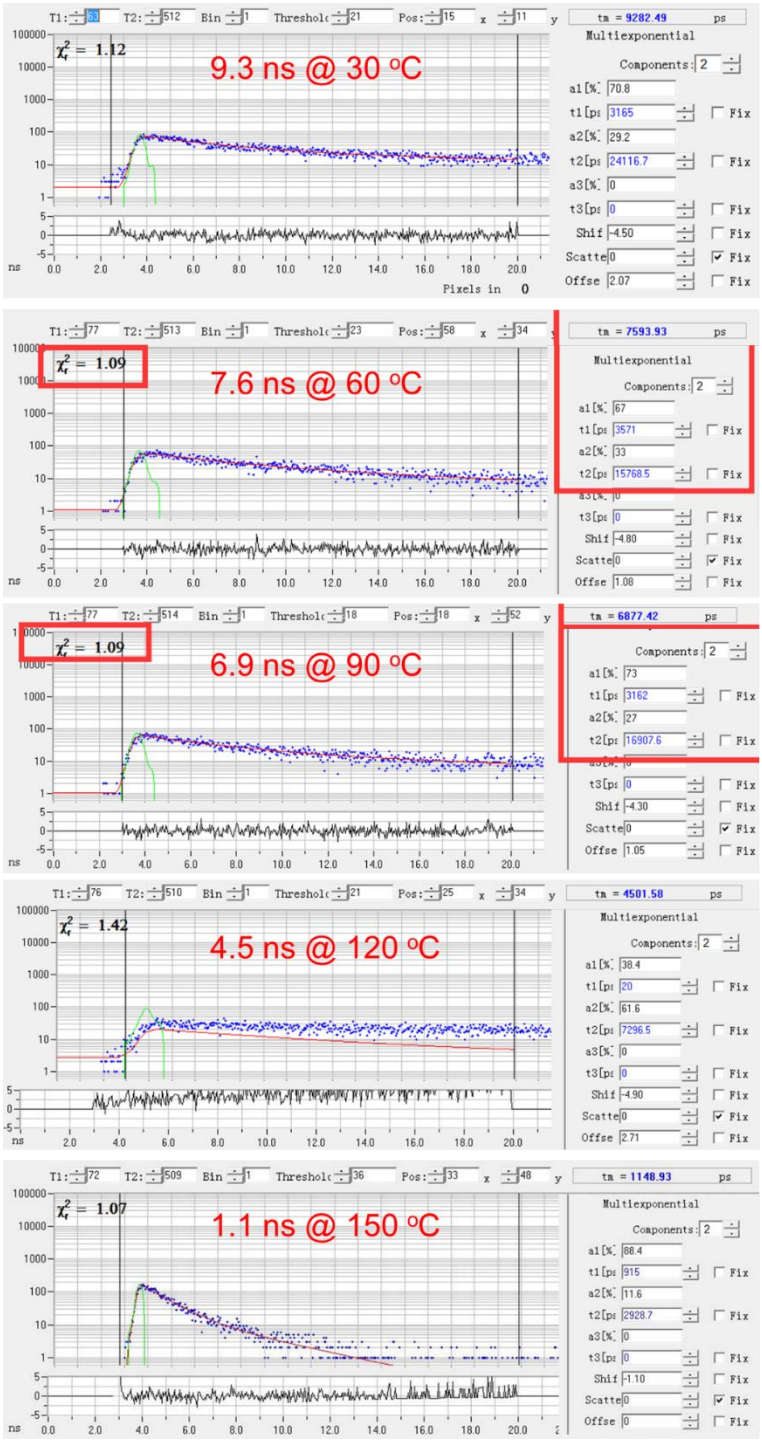

Figure S8. Typical PL decays curve of an interval $CsPbBr_3@Cs_4PbBr_6/SiO_2$ film at various temperatures.

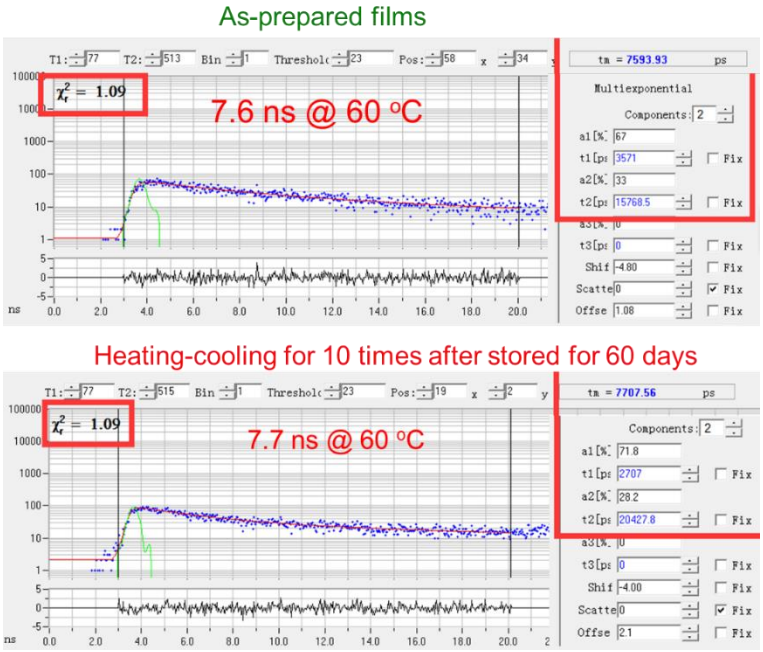

Figure S9. The PL decay curves of $CsPbBr_3@Cs_4PbBr_6/SiO_2$-based film at 60 °C before and after heating-cooling for 10 cycles between 150 °C and 60 °C.

The PL lifetimes of the $CsPbBr_3@Cs_4PbBr_6/SiO_2$-based films at 60 °C before and after heating-cooling for 10 cycles between 150 °C and 60 °C are 6.6, and 6.7 ns, respectively. The PL life time is almost the same, which indicates the fully recover of the heating-cooling process.

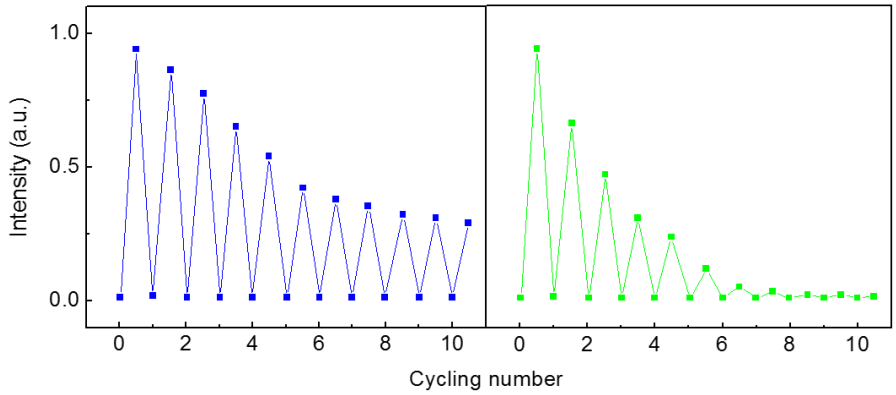

Figure S10. Reversible fluorescent response of 10 consecutive cycles at 30-150 °C of $CsPbBr_3@Cs_4PbBr_6$ and $CsPbBr_3$, respectively.

From Fig.S9, $CsPbBr_3@Cs_4PbBr_6$ and $CsPbBr_3$ exhibit terrible recyclability under heating for the intrinsic quenching in air. Though Cs_4PbBr_6 provide some protection for $CsPbBr_3$, but it's not enough obviously.

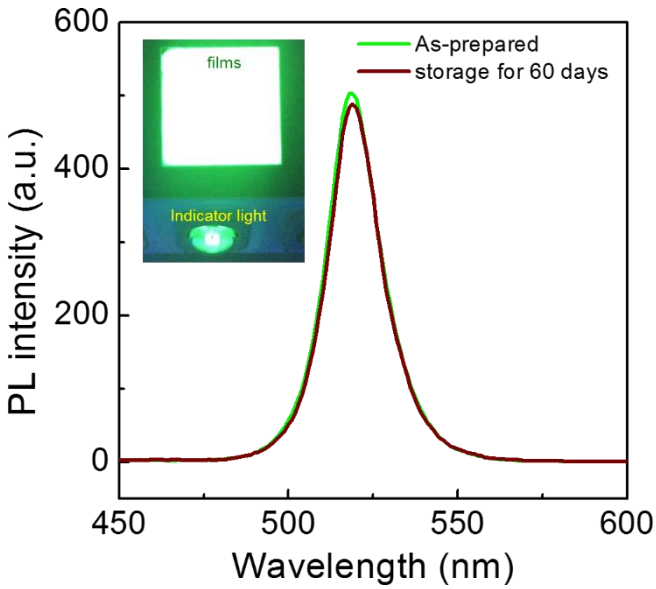

Figure S11. The PL properties of $CsPbBr_3@Cs_4PbBr_6/SiO_2$-based composite films storage for 60 days.

Then PL spectra of Cs_4PbBr_6-based composite films storage for 60 days are almost the same without obvious decrease, which indicated their excellent stability.